Nanoscale

PAPER

View Article Online
View Journal | View Issue

Cite this: *Nanoscale*, 2019, **11**, 3925

On the origins of the green luminescence in the "zero-dimensional perovskite" Cs_4PbBr_6: conclusive results from cathodoluminescence imaging

Nicolas Riesen, *[a,b] Mark Lockrey, [c,d] Kate Badek [e] and Hans Riesen *[e]

Received 16th November 2018,
Accepted 29th January 2019

DOI: 10.1039/c8nr09255a

rsc.li/nanoscale

There is great interest in the use of highly-efficient all-inorganic halide perovskites Cs_nPbBr_{2+n} for optoelectronic applications. There however remains considerable debate as to the origins of the green luminescence in the zero-dimensional phase of the perovskite Cs_4PbBr_6, with theories suggesting it originates either from defects in the Cs_4PbBr_6 lattice or $CsPbBr_3$ impurities/inclusions. The confusion has arisen due to the two phases being miscible and typically co-existing. Moreover, low impurity levels of $CsPbBr_3$ in Cs_4PbBr_6 are difficult to detect by XRD measurements, yet have much stronger photoluminescence than bulk $CsPbBr_3$ that exhibits quenching, further contributing to the confusion as to the origins of the green photoluminescence. With the rise of significant debate and misconceptions, we provide conclusive evidence that the green emission from Cs_4PbBr_6 is indeed due to nanocrystalline $CsPbBr_3$ impurities. This is demonstrated by undertaking cathodoluminescence and EDX measurements on samples prepared mechanochemically by ball-milling. Cathodoluminescence imaging clearly shows the presence of small crystals embedded in/or between larger crystallites of Cs_4PbBr_6 and they emit around 520 nm. EDX shows that the smaller crystal inclusions have a Pb : Br ratio that is approximately 2 times higher, confirming the $CsPbBr_3$ phase, which has the expected size-dependent shift to shorter wavelengths (about 528 to 515 nm). These studies make significant inroads into understanding these lead halide perovskites for their use in a variety of optoelectronic and photovoltaic applications.

Introduction

There is growing interest in the highly-efficient all-inorganic halide perovskites Cs_nPbBr_{2+n} for optoelectronic applications due to their size-tunable bandgaps and superb quantum efficiencies. They also have high stability compared with organic–inorganic hybrids such as $MAPbBr_3$ ($MA = CH_3NH_3^+$).[1] Their increased stability, yet comparable mechanical and optoelectronic properties, could allow for more reliable optoelectronic devices.[1] Perovskites for instance are potential replacements for light-emitting diode CdSe/ZnS QDs,[2] although several issues such as the influence of moisture, feasibility of large scale fabrication and toxicity need to be addressed.[2] This article focuses on the interesting zero-dimensional perovskite phase Cs_4PbBr_6 which crystallizes in the $R\bar{3}c$ (167) space group,[3] where the $PbBr_6$ octahedra are isolated as shown in Fig. 1. The isolation of the octahedra allows for interesting

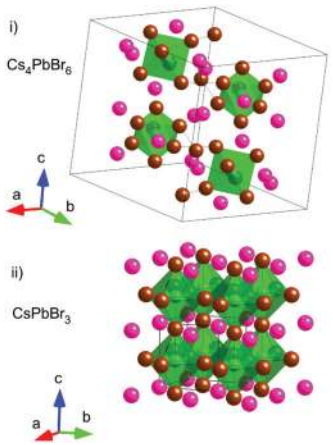

Fig. 1 The (i) Cs_4PbBr_6 structure ($R\bar{3}c$) in comparison with (ii) $CsPbBr_3$ ($Pm\bar{3}m$). Br = brown; Cs = pink; Pb = green. The $PbBr_6$ octahedra are highlighted in translucent green.

[a]*University of South Australia and Future Industries Institute, Mawson Lakes, SA 5095, Australia. E-mail: nicolas.riesen@unisa.edu.au*
[b]*Institute for Photonics and Advanced Sensing (IPAS) and School of Physical Sciences, The University of Adelaide, SA 5005, Australia*
[c]*Research School of Physics & Engineering, The Australian National University, Canberra, ACT 0200, Australia*
[d]*Microstructural Analysis Unit, University of Technology Sydney, PO Box 123, Broadway, NSW 2007, Australia*
[e]*School of Physical, Environmental and Mathematical Sciences, The University of New South Wales, Canberra, ACT 2600, Australia. E-mail: h.riesen@adfa.edu.au*

photophysical properties because of strong quantum confinement and strong exciton–phonon interactions.[4] In contrast, the $CsPbBr_3$ perovskite crystallizes with corner sharing $PbBr_6$ octahedra (see Fig. 1). The latter is the main structural feature that makes $CsPbBr_3$ a relatively narrow band-gap semiconductor.

It is well known that the pure perovskite phase of nanocrystalline $CsPbBr_3$ has photoluminescence emission in the green, whereas the aforementioned zero-dimensional Cs_4PbBr_6 phase emits in the UV with significant debate and misconceptions still existing over whether it too emits in the green at around 520 nm. This debate has gained considerable interest since 2016, with several reports suggesting strong green luminescence from Cs_4PbBr_6 powders,[5,6] whilst interestingly other works reporting an absence of such photoluminescence.[7] Observations of green luminescence from "pure" Cs_4PbBr_6,[2,8–10] have suggested photoluminescence quantum yields (PLQYs) of around 40–50%.[2,8,11,12] This is much higher than that of pure bulk $CsPbBr_3$ which has been observed to have a nearly 2 orders of magnitude lower PLQY.[8] This would seem to suggest that Cs_4PbBr_6 emits in the green, and also more efficiently than $CsPbBr_3$. The reduced efficiency of bulk $CsPbBr_3$ is however due to quenching.[7] Furthermore, colloidal $CsPbBr_3$ can also have PLQYs of around 50% or more,[13] as can a mixture of the two phases.[14] In fact microscale composites of $CsPbBr_3$ nanocrystals in Cs_4PbBr_6 overcome fluorescence quenching of bulk $CsPbBr_3$ because of the quantum confinement, allowing for much higher PLQYs in smaller trace quantities.[15,16] This and the fact that trace quantities of $CsPbBr_3$ in Cs_4PbBr_6 are hard to detect with *e.g.* XRD, has most likely contributed to the misconception that pure Cs_4PbBr_6 emits in the green.

The recent reports of green luminescence in Cs_4PbBr_6 come nearly two decades after it was first observed and discussed in depth in the 1990s by Nikl *et al.*[17] Nikl *et al.* also concluded that unavoidable $CsPbBr_3$ growth is likely the cause for the green photoluminescence in Cs_4PbBr_6. The origin of the green photoluminescence however still remained the subject of much debate after, and especially during the last few years, especially since a proper understanding of this perovskite is critical if it is to be reliably used for light-emitting applications.[9] The two main theories in the literature for the origins of the green photoluminescence have revolved around defects in the Cs_4PbBr_6 lattice,[1,4–6,9,11,18–21] or as we conclude below, $CsPbBr_3$ nanocrystal impurities[14,16,17,22–28] as also originally suggested by Nikl *et al.*[17] Whilst a recent literature review also seems to suggest there is stronger evidence for the theory of $CsPbBr_3$ impurities, further evidence is still needed to decidedly conclude on the origins of the photoluminescence of this interesting material.[7]

The main argument in favour of the presence of $CsPbBr_3$ nanocrystal impurities being the origin of the green luminescence, has been that the different Cs phases (*e.g.* CsBr, Cs_4PbBr_6 and $CsPbBr_3$) are miscible and usually co-exist whilst being very difficult to detect in small quantities, making "pure" Cs_4PbBr_6 appear to emit in the green.[1] The argument against this theory has often made mention of the absence of diffraction peaks of $CsPbBr_3$ in supposedly "pure" Cs_4PbBr_6.[7] As suggested before these peaks are however hard to be detect especially because of the broad width and low intensity of the peaks of small nanocrystals.[22] Furthermore very high PLQY has been demonstrated in Cs_4PbBr_6 matrices with $CsPbBr_3$ nanocrystals encapsulated inside, again suggesting that small traces of the nanocrystals could be enough to yield strong photoluminescence due to the quantum confinement effect.[7] The other argument suggesting that Cs_4PbBr_6 emits in the green typically involves discussion of structural defects, which are known to strongly influence the photoluminescence in 3D and 2D layered perovskites.[7] These may include bromide vacancies or hydroxide impurities. As discussed by Akkerman *et al.*, this is however not quite in agreement with the current understanding of defects in perovskites.[7] Moreover in reports where nucleation or phase transformations to $CsPbBr_3$ have been avoided with oleylamine/ligands, the material is commonly found to be non-emissive.[4,7] Further oddities include the photoluminescence spectrum of "pure" Cs_4PbBr_6 being identical to $CsPbBr_3$ embedded in Cs_4PbBr_6.[29] The peaks of the photoluminescence however strangely always seem to imply a small size range for the $CsPbBr_3$ nanocrystals which could be explained by the way the particles are embedded and protected by the Cs_4PbBr_6 phase. There is also a question mark over whether there might be a synergistic effect at the interface between the two phases resulting in enhanced photoluminescence. Akkerman *et al.*, suggested that further electronic and photoconductivity studies are needed to properly characterize this material and make conclusions on the origins of the green photoluminescence.[7]

In this Article we provide these very studies yielding conclusive evidence that the green emission from Cs_4PbBr_6 is due to nanocrystalline $CsPbBr_3$ impurities. This is achieved by performing cathodoluminescence, EDX and photoluminescence measurements, revealing the real nature of the green emission in Cs_4PbBr_6 perovskites.

Experimental

Cs_4PbBr_6 was prepared by ball-milling stoichiometric mixtures of CsBr (0.4256 g) and $PbBr_2$ (0.1835 g) on a Retsch mixer mill (MM200, zirconia lined 10 ml grinding jar with two 12 mm diameter zirconia balls) at 20 Hz for 90 minutes. The product was then transferred out of the jar into a Petri dish and dried at 50 °C for 30 min with subsequent ball-milling for another 90 min. We note here that the grinding was undertaken in air and hence there were slight variations in ambient humidity and temperature *etc.* from batch to batch that are very difficult to control. For this article we have prepared two batches which are called S1 and S2 below. For the purpose of comparison, we also prepared a $CsPbBr_3$ sample by the same mechanochemical method. Powder X-ray diffraction patterns were obtained on a Rigaku MiniFlex 600 benchtop diffractometer operating at 40 kV and 15 mA with CuKα radiation. Step sizes of 0.01° and 0.005° and scan speeds of 0.25° min^{-1} and 0.06° min^{-1} were

employed for standard and slow scans, respectively. Rietveld refinements were conducted by using the MAUD software package.[30] Room temperature photoluminescence spectra were collected on a conventional fluorometer (Fluoromax-3, Spex Horiba JobinYvon). For reflection spectroscopy, a Shimadzu UV-2450 spectrometer equipped with an ISR-2200 integrating sphere was used with $BaSO_4$ as the reference. The perovskite samples were mixed/diluted into $BaSO_4$ for the reflectance measurements. The transmission electron microscopy (TEM) was performed using a FEI Tecnai G2 Spirit TEM, whereas the optical images were taken on an inverted microscope (IX 71, Olympus, Japan) equipped with suitable dichroic filters. The nanocrystalline samples were excited through the microscope using a 405 nm CW laser source.

Cathodoluminescence measurements of S1 and S2 were performed on a FEI Verios 460 SEM equipped with a Gatan MonoCL4 Elite CL detection system. Full spectral maps were collected using a beam voltage of 5 kV and a current of 200 pA, at room temperature. EDX measurements were collected on the same microscope using an Oxford EDX detector and processed using Aztec. CL measurements on the $CsPbBr_3$ sample were performed using a FEI Quanta 200 SEM using a custom-built CL system. Full spectral mapping was performed with an accelerating voltage of 5 kV and a current of 600 pA.

Results and discussion

In order to characterize the nanocrystals prepared by the mechanochemical method, powder X-ray diffraction measurements were conducted. The powder X-ray pattern of Cs_4PbBr_6 (sample S1) prepared by the ball-milling method, together with a Rietveld refinement is shown in Fig. 2. Typical TEM micrographs of a selection of smaller particles of samples S1 and S2 are shown in panels b and c, respectively, illustrating that the average particle size of S2 is smaller than that of S1.

The lattice parameters resulting from the Rietveld refinement are given in Table 1 and are in good agreement with the published values of 13.71(2) Å and 17.23(7) Å.[31] The Rietveld refinement indicates relatively large average crystallite sizes of 970 ± 100 nm and 260 ± 70 nm for samples S1 and S2, respectively, in the isotropic approximation. It is noted here that the MAUD software package uses the Delft model in a full line-shape analysis for determining the crystallite size, assuming a lognormal crystallite size distribution.[32] The obtained crystallite sizes are in an acceptable agreement with sizes and distributions observed in TEM micrographs.

It appears that the mechanochemical diminution worked better for S2 resulting on average in smaller particles of the Cs_4PbBr_6 phase (as noted above, slight changes in ambient conditions seem to have significant effects on the particle size in the ball-milling process of this material). The Goodness of fit G in the Rietveld refinement is <2 for both samples S1 and S2 validating the crystal structure model.

As is demonstrated in the inset of Fig. 2a, $CsPbBr_3$ can just faintly be detected for S1 and only when using a very slow

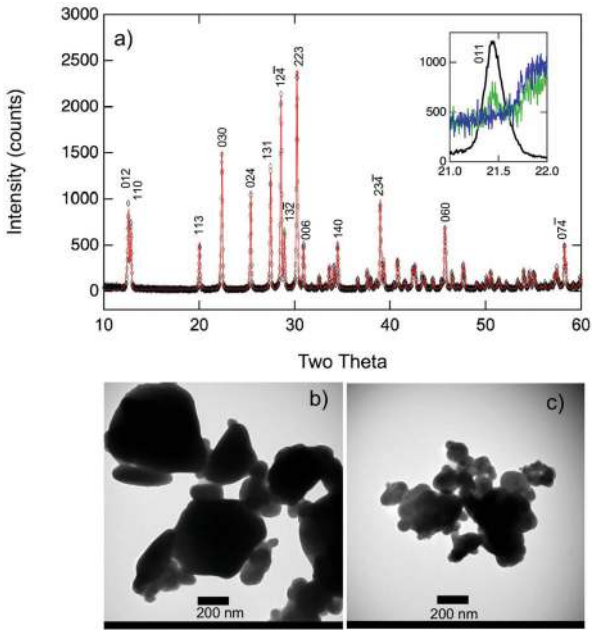

Fig. 2 (a) Powder XRD pattern of Cs_4PbBr_6 (S1) as obtained by the mechanochemical method (black diamonds) in comparison with a Rietveld refinement (red solid line). Miller indices of prominent diffraction peaks are indicated. The inset shows XRD measurements around 21.4° for S1 (green trace, magnified 10×), S2 (blue trace, magnified 10×) and $CsPbBr_3$ (black trace). TEM micrographs (scale bar = 200 nm) for smaller (than average) particles of S1 and S2 are shown in panels (b) and (c), respectively.

scan. It is detected with the appearance of the 011 diffraction peak (note that the traces for S1 and S2 in the inset have been magnified by a factor of 10), which is a prominent diffraction peak of the 3D material at around 21.4°. From these measurements it can be concluded that S1 contains around 1% of the $CsPbBr_3$ phase, whereas in S2 this is <0.2% and not detectable by XRD. We note that the absence of a $CsPbBr_3$ diffraction peak in XRD could easily be mistaken for implying "pure" Cs_4PbBr_6, and this is likely to have caused confusion as to the origins of the green luminescence in the literature as discussed by Akkerman *et al.*[7,22] In the case of impurities on the low nanometer scale, $CsPbBr_3$ inclusions are clearly difficult to detect in the background of an XRD pattern of relatively large crystallites which have much narrower diffraction peaks, even when using a very slow scan.

Fig. 3 shows the green photoluminescence spectra (solid lines) of the two Cs_4PbBr_6 samples with 410 nm excitation in comparison with the emission spectrum of a $CsPbBr_3$ sample previously prepared by ball-milling (average crystallite size of 250 nm).[32] Also shown are the absorption spectra of the three samples (dashed lines), which were obtained by applying the Kubelka–Munk transformation to reflection spectra.

Samples S1 and S2 display luminescence maxima at 527.8 and 519.6 nm with full-widths-at-half-maximum of 20 and 22 nm, respectively. S2 is slightly less luminescent than S1. Although the two samples were nominally prepared by the

Table 1 Lattice parameters and average crystallite size (isotropic approximation) for the two Cs_4PbBr_6 samples obtained by ball-milling. The weighted profile factor R_{wp}, the expected R factor R_{exp} and the Goodness of fit $G = R_{wp}/R_{exp}$ are given

Cs_4PbBr_6	a/Å	c/Å	Av. cryst. size/nm	R_{wp}/%	R_{exp}/%	G
S1	13.7411 (4)	17.3376(6)	970 ± 100	19.8	10.7	1.86
S2	13.7323 (5)	17.3272(8)	260 ± 70	19.1	11.1	1.71

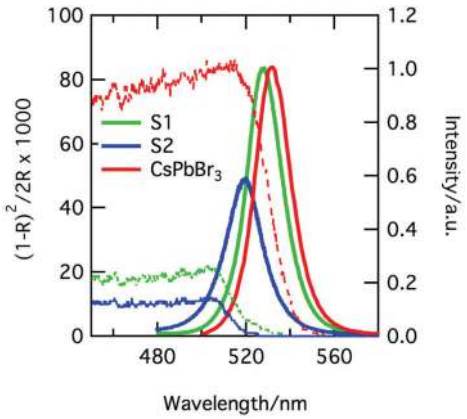

Fig. 3 Photoluminescence (solid lines) and absorption spectra (dashed lines) of Cs_4PbBr_6 samples S1 and S2 prepared by ball-milling. The luminescence (normalized) and absorption spectra of $CsPbBr_3$ (also prepared by ball-milling) are shown for comparison.[33] The luminescence spectra were excited at 410 nm. The absorption spectra were obtained by applying the Kubelka–Munk transformation to reflection spectra. For the latter, samples were diluted with $BaSO_4$.

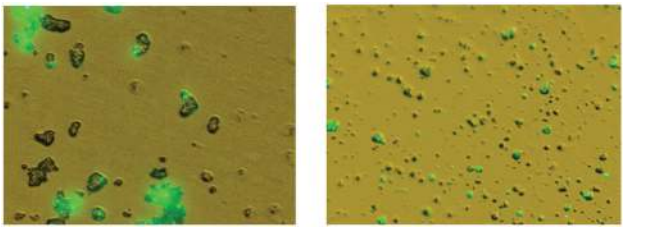

Fig. 4 Microscope images of sample S1 illuminated with a 405 nm laser CW source showing centres of intense green emission. Magnification is 40× and 10×, respectively.

same method, slight variations in the conditions (humidity of air before ball-milling jar was closed, variations in pre-grinding in mortar, drying *etc.*) must have led to slightly different luminescent phases. These conditions are hard to control and further work is needed to gain better control of the preparation method. We note here again that the bulk phase Cs_4PbBr_6 shows different crystallite/particle sizes for the two samples as is discussed above. Fig. 3 also shows the photoluminescence spectrum of $CsPbBr_3$, prepared by the same ball-milling method. Given that the luminescence spectra of S1 and S2 are reminiscent of the $CsPbBr_3$ spectrum (and this has been discussed previously in the literature[29]), Fig. 3 strongly points to the green emission simply being due to $CsPbBr_3$ impurity/inclusions of *different average* particle sizes *i.e.* the $CsPbBr_3$ particles in S2 are apparently significantly smaller than in S1. We note here that the average particle size for the luminescent crystallites in the pure $CsPbBr_3$ phase, prepared by ball-milling, is apparently larger than the ones for the $CsPbBr_3$ impurities in the Cs_4PbBr_6 bulk phase. The absorption spectra obtained *via* reflectance measurements of the powders allowed for determination of the band gap by using the Tauc plot.[34] Band gaps of 2.32 ± 0.01, 2.38 ± 0.01 and 2.42 ± 0.01 eV were obtained from these plots for $CsPbBr_3$, S1 and S2, respectively.

Fig. 4 shows optical images of the green luminescence emission from Sample S1, excited on the inverted microscope. It is obvious that not all crystals are emitting green light as has been observed previously.[7,22]

To provide further evidence on the origins of the green photoluminescence of these perovskites, cathodoluminescence (CL) spectral mapping was used, where a full CL spectrum is collected for each pixel, demonstrating that green-emitting $CsPbBr_3$ impurities/inclusions exist in the Cs_4PbBr_6 bulk phase. Fig. 5 shows SEM plus CL images, and CL spectra for a Cs_4PbBr_6 aggregate of sample S1. There is an obvious bright spot for the 500–540 nm bandpass. This image by itself provides very strong evidence that the green emission in Cs_4PbBr_6 is caused by nanocrystalline $CsPbBr_3$ impurity particles. It is possible that these particles are embedded and hence partially protected by the Cs_4PbBr_6 bulk phase.

The very bright spot in the CL image of Fig. 5e has a very different CL spectrum compared to the rest of the aggregate as is illustrated in panel (g) of Fig. 5. The spectrum of this spot is highly comparable to the PL spectrum shown in Fig. 3 above, and the peak is observed at 521.3 nm with a width of 19 nm indicating a $CsPbBr_3$ particle size that is slightly smaller than the average (see PL spectrum). The EDX measurements illustrated in Fig. 6 in the region of the bright spot corroborate the idea of $CsPbBr_3$ inclusions. Panels (c), (d) and (e) show EDX maps for Pb, Br and Cs. The Pb signal increases across the green luminescence spot whereas no significant change in the Br appears across the map. The Cs signal is too weak, with a S/N ratio of 1, to draw any statistically strong conclusions. A cross-section of the EDX signal across the bright green luminescent spot is shown in panel (f) of Fig. 6. The Pb X-ray fluorescence increases by a factor of about 2, in accord with expectations when crossing from the Cs_4PbBr_6 phase through to the $CsPbBr_3$ phase, whereas the Br signal only increases very slightly. The weight% ratio Pb/Br as obtained from these measurements is shown in Fig. 6f corroborating the $CsPbBr_3$ phase in the green luminescent spot. It is noted here that the

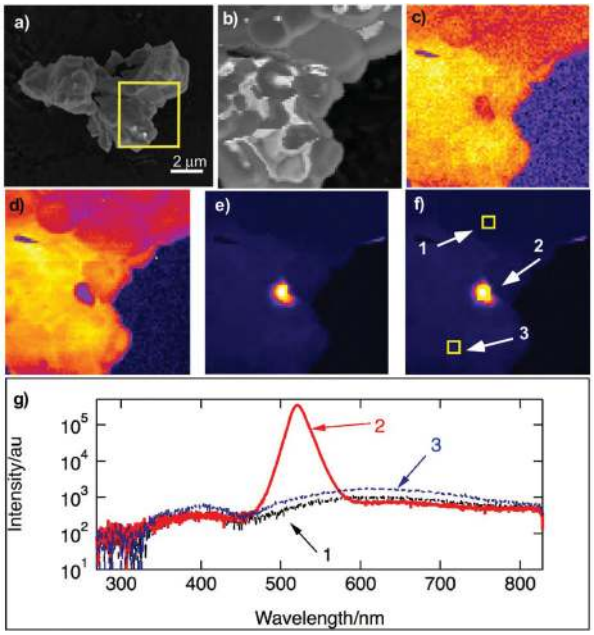

Fig. 5 (a) SEM micrograph and (b) zoomed in region (square window in a) of a large particle aggregate of Cs_4PbBr_6 (S1) with CL bandpass images (c) 340–450 nm, (d) 600–700 nm and (e),(f) 500–540 nm. (f) Indicates the areas from which the CL spectra shown in panel (g) were extracted.

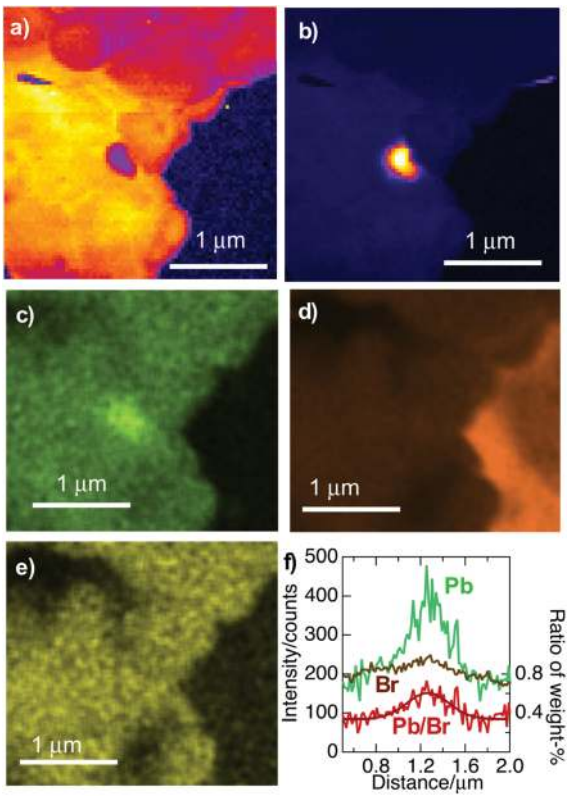

Fig. 6 CL bandpass images: (a) 600–700 nm, (b) 500–540 nm. EDX maps of (c) Pb (M lines), (d) Br (L lines) and (e) Cs (M lines). (f) EDX signals from the Pb (M lines) and Br (L lines, scaled to the Pb raw signal) across the bright green luminescent spot, and EDX weight% ratio Pb/Br.

EDX measurements will be affected to some extent if the $CsPbBr_3$ nanoparticles are embedded *i.e.* the signal will depend on the depth of embedment. Although the EDX signal for Cs is weak with a S/N ratio of 1, a decrease of the signal can be observed across the green luminescent spot.

In Fig. 7 CL images with 340–450, 500–540 and 600–700 nm band passes are shown for another aggregate of sample S1. Again, a very bright spot dominates the green emission (500–540 nm). Measuring the CL spectra in 3 regions as indicated where there is green emission, a sizeable wavelength shift is observed. Spot 1 shows very weak luminescence at around 518 nm and spots 2 and 3 show emissions peaking at 519.3 and 523.5 nm, respectively. The luminescence at spot 2 is about 10× weaker than the one of spot 3. The wavelength shift to shorter wavelengths is commensurate with the intensity being dependent on the $CsPbBr_3$ impurity particle size.

Fig. 8 summarizes the CL images of the Cs_4PbBr_6 sample S2 in comparison with the SEM micrograph. It is noted here that for this sample the percentage of particles that show 520 nm emission is more limited than for S1 in accord with the observation that S2 displays lower photoluminescence intensity than S1. When observing CL with a 500–540 nm bandpass, very small bright spots are observed (white arrow 1

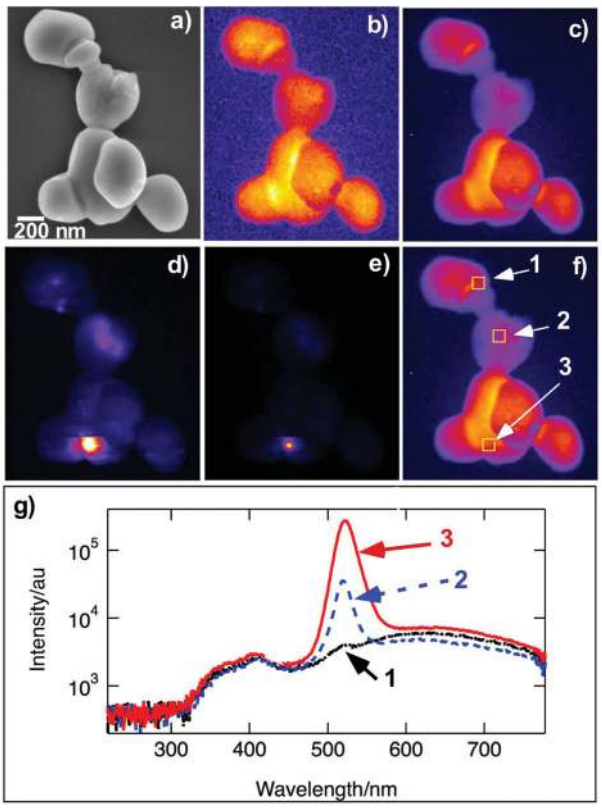

Fig. 7 SEM micrograph of a particle aggregate of Cs_4PbBr_6 (S1) with CL bandpass images (b) 340–450 nm, (c) 600–700 nm and (d), (e) 500–540 nm. (f) Indicates the areas of which the CL spectra shown in (g) were measured. The CCD was saturated at the bright spot of the CL image (d).

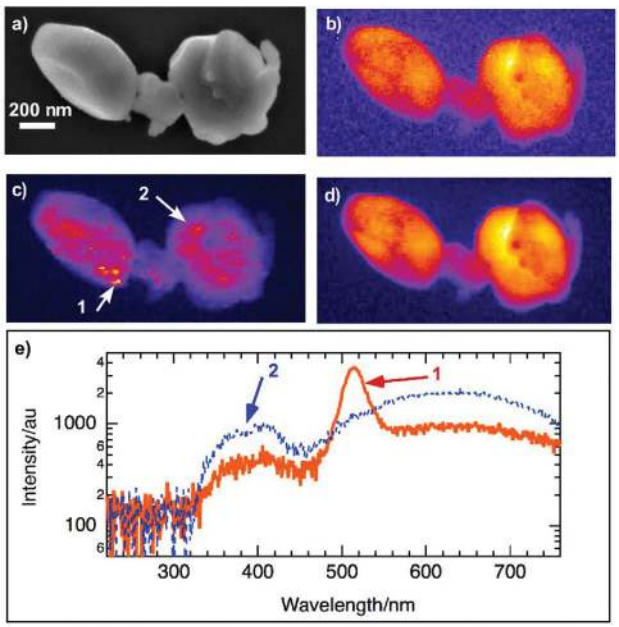

Fig. 8 (a) SEM micrograph of a particle aggregate of Cs_4PbBr_6 (S2) with CL bandpass images (b) 340–450 nm, (c) 500–540 nm and (d) 600–700 nm. (c) Indicates the areas where the CL spectra shown in (e) were extracted from.

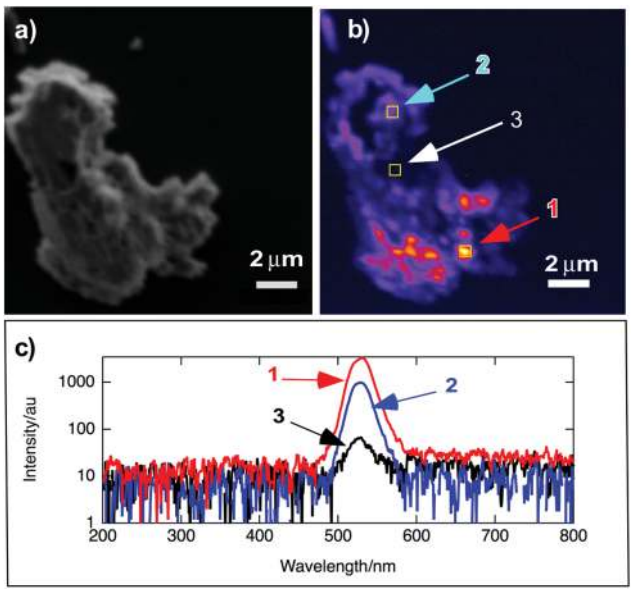

Fig. 9 (a) SEM micrograph of $CsPbBr_3$ aggregate with (b) CL image (500–560 nm bandpass) and (c) CL spectra for three regions.

in c). These spots are on or below the scale of the step size of the CL imaging *i.e.* 10 nm.

Fig. 8(e) shows CL spectra of the bright spot 1 in comparison with the spectrum extracted from spot 2. Very obvious again is that the bright spot is based on $CsPbBr_3$. The observed peak maximum of 515.5 nm indicates that these embedded particles are very small in accord with the PL and absorption spectra in Fig. 3 above.

Therefore, cathodoluminescence imaging has clearly shown that nanocrystals embedded in/or between larger crystallites of Cs_4PbBr_6 are those that are luminescent around 520 nm. EDX shows that the luminescent particles/crystallites have a Pb : Br ratio that is about 2× higher *i.e.* confirming the $CsPbBr_3$ phase. In addition, smaller crystallites of this phase show the expected shift to shorter wavelength (about 528 to 515 nm).

Neglecting polarization terms, the particle size of the embedded $CsPbBr_3$ phase can be estimated by using eqn (1).[35,36]

$$E(R) = E_g + \frac{\hbar^2\pi^2}{2\mu^* R^2} - 1.8\frac{e^2}{4\pi\varepsilon_0\varepsilon_r R} \quad (1)$$

where E_g is the band gap of the bulk material, R is the radius of the nanoparticle and μ^* is the effective reduced mass of the exciton. Protesescu *et al.*[13] determined a value of $\mu^* = 0.07m_e$ (m_e = mass of electron) and the energy gap of the bulk has been reported to be ~2.3 eV,[37] in good agreement with the 2.32 eV obtained by reflectance measurements presented above. The second term in eqn (1) is just the zero-point energy (kinetic energy) of a particle in a sphere of radius R. The third term in eqn (1) accounts for the screened Coulomb interaction between the electron and the hole. Using eqn (1) and a comparison with the results of ref. 36 and 38 we estimate, crudely, a range of embedded $CsPbBr_3$ particle sizes between 30 and 8 nm. In particular for sample S1 and S2, the average particle sizes are ~15 nm (E = 2.38 eV) and ~12 nm (E = 2.42 eV), respectively. This is commensurate with rough estimates from CL images. It appears that the photoluminescence spectra are red shifted compared to the maxima observed for colloidal nanocrystals. This may be due to some clustering of $CsPbBr_3$ nanocrystals in the Cs_4PbBr_6 bulk phase resulting in excitation energy transfer to lower energy. The PL maxima are reminiscent of nanocrystalline $CsPbBr_3$ films with similar crystallite sizes.[39] The latter is plausible given that the present measurements were all conducted with samples in powder form. Further work is however needed to fully understand the red shift.

Finally, the question arises as to whether the luminescence in $CsPbBr_3$ prepared by ball-milling is also due to $CsPbBr_3$ nanocrystals embedded into the bulk phase. As Fig. 9 shows this is indeed the case with bright spots again being observed representing $CsPbBr_3$ nanoparticles embedded into the $CsPbBr_3$ bulk phase with the latter having a very low PLQY. Interestingly, the energy difference between the absorption edge and the photoluminescence maximum is less than that for S1 and S2. This is because the absorption in the case of $CsPbBr_3$ is caused by the $CsPbBr_3$ bulk phase whereas the absorption in S1 and S2 around 520 nm is caused by the $CsPbBr_3$ nanocrystals embedded in the Cs_4PbBr_6 phase.

Conclusions

We studied the origins of the green photoluminescence from the lead halide perovskite Cs_4PbBr_6, providing conclusive

evidence using cathodoluminescence imaging and spectroscopy and EDX that the green photoluminescence actually originates from $CsPbBr_3$ nanocrystalline impurities or inclusions that are miscible and typically co-exist. It is likely these nanocrystalline impurities are well embedded into the Cs_4PbBr_6 bulk phase and hence are to a great extent protected. EDX shows that the luminescent inclusions have a Pb : Br ratio that is about 2× higher *i.e.* confirming the $CsPbBr_3$ phase. Smaller crystallites (or clusters of nanocrystallites) of this phase show the expected shift to shorter wavelength (from about 528 to 515 nm). These studies make significant inroads into understanding these lead halide perovskites so that they may be used for optoelectronic and photovoltaic applications such as solar cells, colour converters, lasers and light-emitting diodes.[2] The present work also points to the potential of using mechanochemical methods for the tailored preparation of highly luminescent Cs_4PbBr_6 mixtures with nanocrystalline $CsPbBr_3$ impurities. The present article also strongly corroborates the power of cathodoluminescence imaging for the elucidation of the nature of luminescent nanostructures.[40] In particular, CL imaging and spectroscopy appear to be a very powerful tool to analyse the spatial distribution and correlation of luminescence in lead halide nanosystems.

Conflicts of interest

There are no conflicts to declare.

Acknowledgements

N. R. acknowledges the support of an Australian Research Council (ARC) Laureate Fellowship awarded to Tanya M. Monro. This work has been made possible through access to the ACT Node of the Australian National Fabrication Facility (ANFF).

Notes and references

1 Y. Rakita, N. Kedem, S. Gupta, A. Sadhanala, V. Kalchenko, M. L. Böhm, M. Kulbak, R. H. Friend, D. Cahen and G. Hodes, *Cryst. Growth Des.*, 2016, **16**, 5717–5725.
2 Y. H. Song, S. H. Choi, W. K. Park, J. S. Yoo, S. B. Kwon, B. K. Kang, S. R. Park, Y. S. Seo, W. S. Yang and D. H. Yoon, *Sci. Rep.*, 2018, **8**, 2009.
3 C. K. Møller, *On the structure of cæsium hexahalogeno-plumbates (2)*, Ejnar Munksgaard i komm, 1960.
4 J. Yin, Y. Zhang, A. Bruno, C. Soci, O. M. Bakr, J.-L. Brédas and O. F. Mohammed, *ACS Energy Lett.*, 2017, **2**, 2805–2811.
5 M. Saidaminov, J. Almutlaq, S. Sarmah, I. Dursun, A. A. Zhumekenov, R. Begum, J. Pan, N. Cho, O. F. Mohammed and O. M. Bakr, *ACS Energy Lett.*, 2016, **1**, 840–845.
6 D. Chen, Z. Wan, X. Chen, Y. Yuan and J. Zhong, *J. Mater. Chem. C*, 2016, **4**, 10646–10653.
7 Q. A. Akkerman, A. L. Abdelhady and L. Manna, *J. Phys. Chem. Lett.*, 2018, **9**, 2326–2337.
8 M. I. Saidaminov, J. Almutlaq, S. Sarmah, I. Dursun, A. A. Zhumekenov, R. Begum, J. Pan, N. Cho, O. F. Mohammed and O. M. Bakr, *ACS Energy Lett.*, 2016, **1**, 840–845.
9 H. Zhang, Q. Liao, Y. Wu, J. Chen, Q. Gao and H. Fu, *Phys. Chem. Chem. Phys.*, 2017, **19**, 29092–29098.
10 B. Billstrand, K. Bian, C. Karler, D. Ye, A. Hwang and H. Fan, *MRS Adv.*, 2018, 1–7.
11 Y. Zhang, L. Sinatra, E. Alarousu, J. Yin, A. M. El-Zohry, O. M. Bakr and O. F. Mohammed, *J. Phys. Chem. C*, 2018, **122**, 6493–6498.
12 X. Chen, D. Chen, J. Li, G. Fang, H. Sheng and J. Zhong, *Dalton Trans.*, 2018, **47**, 5670–5678.
13 L. Protesescu, S. Yakunin, M. I. Bodnarchuk, F. Krieg, R. Caputo, C. H. Hendon, R. X. Yang, A. Walsh and M. V. Kovalenko, *Nano Lett.*, 2015, **15**, 3692–3696.
14 X. Chen, F. Zhang, Y. Ge, L. Shi, S. Huang, J. Tang, Z. Lv, L. Zhang, B. Zou and H. Zhong, *Adv. Funct. Mater.*, 2018, **28**, 1706567.
15 T. Xuan, S. Lou, J. Huang, L. Cao, X. Yang, H. Li and J. Wang, *Nanoscale*, 2018, **10**, 9840–9844.
16 B. Kang and K. Biswas, *J. Phys. Chem. Lett.*, 2018, **9**, 830–836.
17 M. Nikl, E. Mihokova, K. Nitsch, F. Somma, C. Giampaolo, G. Pazzi, P. Fabeni and S. Zazubovich, *Chem. Phys. Lett.*, 1999, **306**, 280–284.
18 Y. Zhang, M. I. Saidaminov, I. Dursun, H. Yang, B. Murali, E. Alarousu, E. Yengel, B. A. Alshankiti, O. M. Bakr and O. F. Mohammed, *J. Phys. Chem. Lett.*, 2017, **8**, 961–965.
19 M. De Bastiani, I. Dursun, Y. Zhang, B. A. Alshankiti, X.-H. Miao, J. Yin, E. Yengel, E. Alarousu, B. Turedi, J. M. Almutlaq, M. I. Saidaminov, S. Mitra, I. Gereige, A. AlSaggaf, Y. Zhu, Y. Han, I. S. Roqan, J.-L. Bredas, O. F. Mohammed and O. M. Bakr, *Chem. Mater.*, 2017, **29**(17), 7108–7113.
20 S. Seth and A. Samanta, *J. Phys. Chem. Lett.*, 2017, **9**, 176–183.
21 R. Andrews, S. Clark, J. Donaldson, J. Dewan and J. Silver, *Chem. Informationsdienst*, 1983, **14**, DOI: 10.1002/chin.198328018.
22 Q. A. Akkerman, S. Park, E. Radicchi, F. Nunzi, E. Mosconi, F. De Angelis, R. Brescia, P. Rastogi, M. Prato and L. Manna, *Nano Lett.*, 2017, **17**, 1924–1930.
23 J. Xu, W. Huang, P. Li, D. R. Onken, C. Dun, Y. Guo, K. B. Ucer, C. Lu, H. Wang and S. M. Geyer, *Adv. Mater.*, 2017, **29**, 1703703.
24 M. Hu, C. Ge, J. Yu and J. Feng, *J. Phys. Chem. C*, 2017, **121**, 27053–27058.
25 C. de Weerd, J. Lin, L. Gomez, Y. Fujiwara, K. Suenaga and T. Gregorkiewicz, *J. Phys. Chem. C*, 2017, **121**, 19490–19496.
26 L. Yang, D. Li, C. Wang, W. Yao, H. Wang and K. Huang, *J. Nanopart. Res.*, 2017, **19**, 258.
27 S. Kondo, K. Amaya and T. Saito, *J. Phys.: Condens. Matter*, 2002, **14**, 2093.

28 M. Velázquez, A. Ferrier, S. Péchev, P. Gravereau, J.-P. Chaminade, X. Portier and R. Moncorgé, *J. Cryst. Growth*, 2008, **310**, 5458–5463.
29 Y. Wang, D. Yu, Z. Wang, X. Li, X. Chen, V. Nalla, H. Zeng and H. Sun, *Small*, 2017, **13**, 1701587.
30 http://maud.radiographema.eu/.
31 R. H. Andrews, S. J. Clark, J. D. Donaldson, J. C. Dewan and J. Silver, *J. Chem. Soc., Dalton Trans.*, 1983, 767–770.
32 D. Balzar, N. Audebrand, M. Daymond, A. Fitch, A. Hewat, J. Langford, A. Le Bail, D. Louër, O. Masson and C. N. McCowan, *J. Appl. Crystallogr.*, 2004, **37**, 911–924.
33 J. Zhang, N. Riesen, L. T. Kasim, K. Badek and H. Riesen, *J. Mater. Sci.*, 2018, **53**, 13643–13659.
34 J. Tauc, *Mater. Res. Bull.*, 1968, **3**, 37–46.
35 L. E. Brus, *J. Chem. Phys.*, 1984, **80**, 4403–4409.
36 L. Brus, *J. Phys. Chem.*, 1986, **90**, 2555–2560.
37 J. Liang, C. Wang, Y. Wang, Z. Xu, Z. Lu, Y. Ma, H. Zhu, Y. Hu, C. Xiao and X. Yi, *J. Am. Chem. Soc.*, 2016, **138**, 15829–15832.
38 B. Ai, C. Liu, Z. Deng, J. Wang, J. Han and X. Zhao, *Phys. Chem. Chem. Phys.*, 2017, **19**, 17349–17355.
39 Q. A. Akkerman, S. G. Motti, A. R. Srimath Kandada, E. Mosconi, V. D'Innocenzo, G. Bertoni, S. Marras, B. A. Kamino, L. Miranda and F. De Angelis, *J. Am. Chem. Soc.*, 2016, **138**, 1010–1016.
40 M. A. Stevens-Kalceff, Z. Liu and H. Riesen, *Microsc. Microanal.*, 2012, **18**, 1229–1238.